

On the model uncertainties for the predicted muon content of extensive air showers

Sergey Ostapchenko and Günter Sigl

Universität Hamburg, II Institut für Theoretische Physik, 22761 Hamburg, Germany

April 3, 2024

Abstract

Motivated by the excess of the muon content of cosmic ray induced extensive air showers (EAS), relative to EAS modeling, observed by the Pierre Auger Observatory, and by the tension between Auger data and air shower simulations on the maximal muon production depth X_{\max}^{μ} , we investigate the possibility to modify the corresponding EAS simulation results, within the Standard Model of particle physics. We start by specifying the kinematic range for secondary hadron production, which is of relevance for such predictions. We further investigate the impact on the predicted EAS muon number and on X_{\max}^{μ} of various modifications of the treatment of hadronic interactions, in the framework of the QGSJET-III model, in particular the model calibration to accelerator data, the amount of the “glue” in the pion, and the energy dependence of the pion exchange process. None of the considered modifications of the model allowed us to enhance the EAS muon content by more than 10%. On the other hand, for the maximal muon production depth, some of the studied modifications of particle production give rise up to ~ 10 g/cm² larger X_{\max}^{μ} values, which increases the difference with Auger observations.

1 Introduction

Experimental studies of very high energy cosmic rays (CRs) are traditionally performed using extensive air shower (EAS) techniques: measuring various characteristics of nuclear-electromagnetic cascades initiated by interactions of primary CR particles in the atmosphere [1]. Such investigations necessarily involve an extensive use of numerical simulation tools designed to describe the EAS development [2]. An accurate reconstruction of the properties of CR primaries depends thus strongly on the precision of air shower modeling. This is especially so for CR composition studies since the relevant EAS characteristics are governed by interactions with air nuclei both of primary CR particles and of secondary hadrons produced in the shower cascade process. Consequently, a successful determination of the primary CR composition is only possible if such hadronic interactions are correctly described by the corresponding Monte Carlo (MC) generators.

One of the traditional methods for CR composition studies relies on measurements of the muon component of air showers by ground-based detectors. However, for ultra-high energy cosmic rays (UHECRs), the use of that technique remained hampered for nearly two decades by the persistent contradiction between experimental observations and EAS simulations, regarding the muon number at observation levels [3, 4, 5, 6], the discrepancy reaching 50% level. Using present air shower simulation tools, the observed muon number N_{μ} would correspond to primary particles being as heavy as uranium nuclei, which, given the exceedingly rare natural abundance of such nuclei, appears very unlikely. A number of theoretical approaches potentially capable to resolve this so-called “muon puzzle” [7] has been proposed, typically advocating to physics beyond the Standard Model [8, 9, 10, 11]. However, since such suggestions are of a rather speculative character, it may

be important to perform a quantitative study of the uncertainty range for the predicted EAS muon content, within the standard physics picture.

Such an investigation is the subject of the current work. Using the recently developed QGSJET-III model [12, 13], we study the dependence of the predicted N_μ on uncertainties regarding the model calibration to relevant accelerator data and on possible changes of the underlying theoretical mechanisms. In addition to the total muon number at ground level, we consider also the maximal muon production depth X_{\max}^μ measured by the Pierre Auger Observatory [14, 15], for which significant discrepancies with predictions of EAS simulations have also been observed. Compared to previous studies of uncertainties of EAS predictions (e.g. [16]), our investigation differs in three key aspects: i) the changes of the corresponding modeling are performed at a microscopic level; ii) the considered modifications are restricted by the requirement not to contradict basic physics principles; iii) the consequences of such changes, regarding a potential (dis)agreement with relevant accelerator data, are analyzed.

The paper is organized as follows. In Section 2, we study the kinematic range for secondary hadron production, which is of relevance to N_μ and X_{\max}^μ predictions, using the QGSJET-II-04 [17, 18], EPOS-LHC [19], and SIBYLL-2.3 [20] MC generators. In Section 3, we consider potential variations both of the parameters and of the underlying theoretical mechanisms of the QGSJET-III model, while checking the corresponding impact on the predicted N_μ and X_{\max}^μ . Finally, we discuss our results and conclude in Section 4.

2 Kinematics of secondary hadron production, relevant to N_μ and X_{\max}^μ predictions

The muon component of extensive air showers is formed by a long nuclear cascade in the atmosphere, primarily driven by pion-air interactions.¹ It is thus evident that the multiplicity of secondary pions or, more generally, of all kinds of relatively stable hadrons (i.e., those whose interaction length in the atmosphere is substantially shorter than the decay length), has a direct impact on the expected muon signal at ground, which can be qualitatively understood using the simple Heitler's picture of the cascade process [21] (see also [22]). A more delicate question addressed, e.g., in [23] (see also [24] for a recent study) is what range of energy fractions taken by secondary pions from their parent hadrons, $x_E = E/E_0$, is of highest importance for the predicted N_μ . On the one side, secondary hadron production in high energy collisions is spread over the whole available rapidity range, $0 < y < \ln s$, in the laboratory (lab.) frame, s being the center-of-mass (c.m.) energy squared for the collision. Hence, the bulk of secondaries is characterized by vanishingly small $x_E \propto e^y/s$. On the other hand, interactions of most energetic secondary hadrons initiate powerful enough subcascades, thereby providing a higher contribution to the observed N_μ . The competition between these two trends can be easily quantified considering, for the moment, only contributions of pion-air interactions and making a rather reasonable assumption, being again motivated by Heitler's picture, that the energy-dependence of the muon content of a nuclear subcascade initiated by a charged pion can be approximated by a power law:

$$N_\mu^{\pi^\pm}(E_0) \propto E_0^{\alpha_\mu}. \quad (1)$$

Under these assumptions, N_μ of a proton-initiated air shower is given as

$$N_\mu^p(E_0) \propto \int dx_E \frac{dn_{p\text{-air}}^{\pi^\pm}(E_0, x_E)}{dx_E} N_\mu^{\pi^\pm}(x_E E_0), \quad (2)$$

with $dn_{p\text{-air}}^{\pi^\pm}(E_0, x_E)/dx_E$ being the x_E distribution of secondary charged pions in a proton-air

¹Since the multiplicity of secondary kaons in hadron-nucleus and nucleus-nucleus collisions is about 10% of that of pions, kaon-air interactions play a somewhat subdominant role.

collision at lab. energy E_0 . Such a distribution can be approximated as

$$\frac{dn_{p\text{-air}}^{\pi^\pm}(E_0, x_E)}{dx_E} \propto x_E^{-1-\Delta(E_0)} (1-x_E)^{\beta(E_0)}, \quad (3)$$

within the differences between the predictions of current MC generators, as illustrated in Fig. 1 for the case of a proton-nitrogen (pN) collision at $E_0 = 10^{17}$ eV.

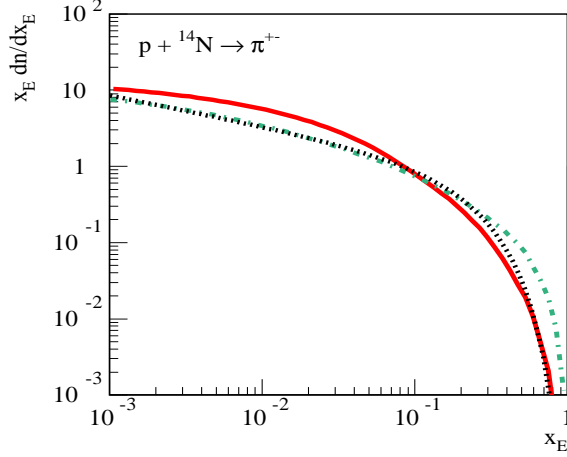


Figure 1: x_E distribution of charged pions for pN collision, $x_E dn_{pN}^{\pi^\pm}/dx_E$, at $E_0 = 10^{17}$ eV, as calculated using the QGSJET-II-04 (solid line) and SIBYLL-2.3 (dash-dotted line) models. Shown by the dotted line is the approximation of the SIBYLL-2.3 results, using the ansatz of Eq. (3), with $\Delta = 0.4$ and $\beta = 4.5$.

Inserting Eq. (3) into Eq. (2) and making use of Eq. (1), we have immediately

$$N_\mu^p(E_0) \propto E_0^{\alpha_\mu} \int dx_E x_E^{\alpha_\mu-1-\Delta(E_0)} (1-x_E)^{\beta(E_0)}. \quad (4)$$

From Eq. (4), we get the “average” $\langle x_E^\pi \rangle$ for p -air interactions, weighted by the contributions of the corresponding pion subcascades to N_μ :

$$\langle x_E^\pi \rangle = \frac{\int_0^1 dx_E x_E^{\alpha_\mu-\Delta} (1-x_E)^\beta}{\int_0^1 dx_E x_E^{\alpha_\mu-1-\Delta} (1-x_E)^\beta} = \frac{\alpha_\mu - \Delta}{1 + \alpha_\mu + \beta - \Delta}. \quad (5)$$

For $\alpha_\mu \simeq 0.9$, using the parameters of the fit in Fig. 1, $\Delta = 0.4$ and $\beta = 4.5$, we get $\langle x_E^\pi \rangle \simeq 0.1$. In Fig. 2, we plot the cumulative x_E distribution,

$$F(x_E) = \frac{\int_0^{x_E} dx x^{\alpha_\mu-1-\Delta} (1-x)^\beta}{\int_0^1 dx x^{\alpha_\mu-1-\Delta} (1-x)^\beta}, \quad (6)$$

for these parameter values. As one can see in the Figure, only 1/4 of the contribution comes from the interval $x_E < 0.01$. The same reasoning can be repeated for pion-air collisions, if we neglect the diffractive contribution which, as will be demonstrated in the following, is of minor importance for N_μ , yielding a similarly large value for $\langle x_E^\pi \rangle$.

Thus, the air shower muon content is governed by forward pion production in hadron-air collisions, at the many steps of the nuclear cascade in the atmosphere. Let us further support this conclusion by a numerical study, using a number of popular MC generators of CR interactions. To this end, we modify pion energy distributions provided by those models, replacing every second

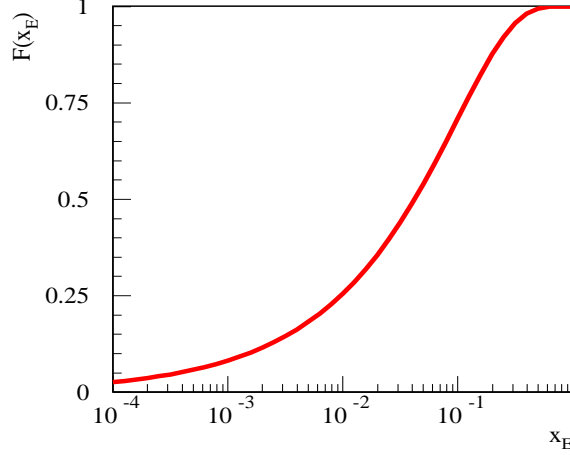


Figure 2: Cumulative x_E distribution, Eq. (6), for $\Delta = 0.4$, $\beta = 4.5$, and $\alpha_\mu = 0.9$.

pion characterized by energy fraction x_E bigger than some cutoff x_{cut} by a pair of pions of half the energy. Importantly, doing so, we replace a charged pion by a pair of charged pions, while a π^0 is being “split” into a pair of neutral pions, such that the energy partition between nuclear and electromagnetic (e/m) cascades remains unaltered in average.

The modifications of secondary pion energy distributions by such a procedure are exemplified in Fig. 3. For large $x_{\text{cut}} \simeq 1$, this impacts the diffractive peak only, leaving a half of it; such a

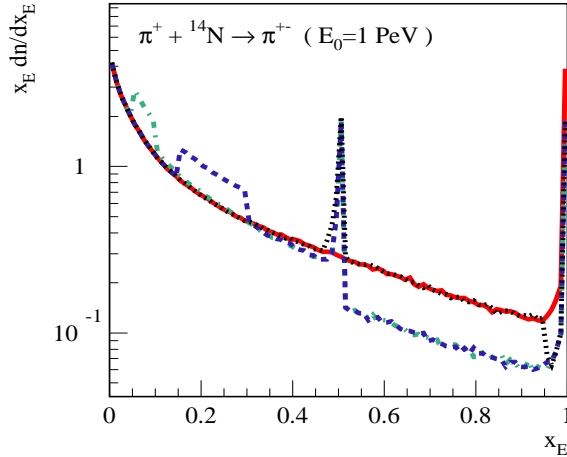


Figure 3: x_E distribution of charged pions for π^+N collision, $x_E dn_{\pi^+}/dx_E$, at $E_0 = 1$ PeV, as calculated using the QGSJET-II-04 model (solid line). The modifications of this distribution by the “splitting” procedure discussed in the text are shown by the dotted, dashed, and dash-dotted lines for $x_{\text{cut}} = 0.95, 0.3$, and 0.1 , respectively.

peak reappears then at $x_E \simeq 0.5$. Choosing a smaller x_{cut} , a larger and larger part of the very forward pion spectrum is reduced, being accompanied by an enhancement of pion production at smaller x_E . In the limit $x_{\text{cut}} \rightarrow 0$, the forward pion production is reduced considerably, while the total multiplicity of secondary pions is increased by 50%.

In Fig. 4, we plot the x_{cut} dependence of the relative change of the calculated N_μ ($E_\mu > 1$ GeV) at sea level, $\Delta N_\mu/N_\mu$, for p -induced EAS of $E_0 = 10^{19}$ eV, applying such a “splitting” procedure

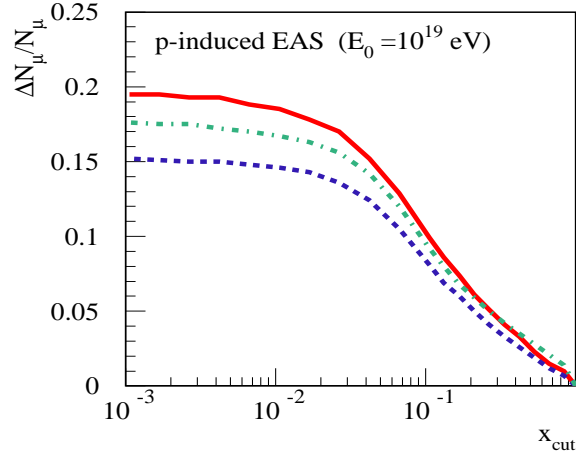


Figure 4: x_{cut} dependence of the relative change of N_μ ($E_\mu > 1$ GeV) at sea level, for p -induced EAS of $E_0 = 10^{19}$ eV, for the pion “splitting” procedure, for different interaction models: QGSJET-II-04 (solid line), EPOS-LHC (dashed line), and SIBYLL-2.3 (dash-dotted line).

to all hadron-air interactions in the shower,² which are treated by the QGSJET-II-04, EPOS-LHC, or SIBYLL-2.3 models. The first thing to notice is that for x_{cut} values close to unity, there is practically no change of N_μ , i.e., pion diffraction is rather irrelevant for EAS muon content. Secondly, the largest gradient of the $\Delta N_\mu(x_{\text{cut}})$ dependence is observed for $x_{\text{cut}} \sim 0.1$, thereby supporting our previous estimation, Eq. (5). In the limit $x_{\text{cut}} \rightarrow 0$, the EAS muon content is enhanced by $\sim 15 - 20\%$, depending on the interaction model. It should be stressed, however, that the performed study serves illustrative purposes only, not being a viable procedure for modifying the predicted N_μ . For example, when the discussed “splitting” is applied to half the secondary pions (the case $x_{\text{cut}} \rightarrow 0$), one arrives to a strong contradiction with available accelerator data. This is illustrated in Fig. 5, where we plot momentum distributions of charged pions, for π^-C collisions

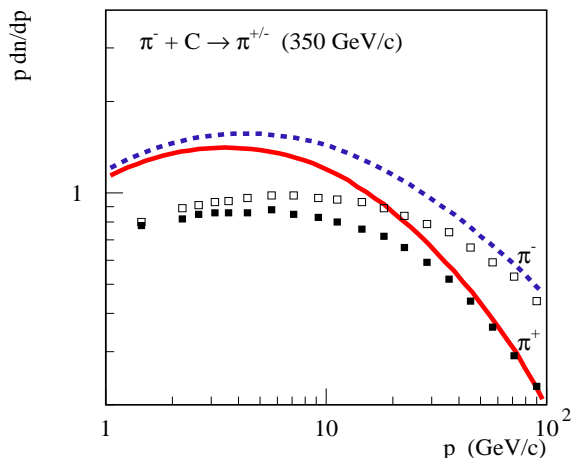


Figure 5: Momentum distributions (in lab. frame) of charged pions produced in π^-C collisions at 350 GeV/c, obtained using the QGSJET-II-04 model and applying the “splitting” procedure to half the secondary pions, compared to NA61 data [26] (points): π^+ – solid line and filled squares, π^- – dashed line and open squares.

²Here and in the following, we perform EAS simulations, using the CONEX code [25].

at 350 GeV/c, obtained using the QGSJET-II-04 model and applying the “splitting” procedure to half the secondary pions (the case $x_{\text{cut}} = 0$), in comparison to NA61 data [26].

The same kind of analysis has been performed for the maximal muon production depth X_{max}^μ , the obtained $\Delta X_{\text{max}}^\mu(x_{\text{cut}})$ dependence being plotted in Fig. 6, again for p -induced EAS of $E_0 =$

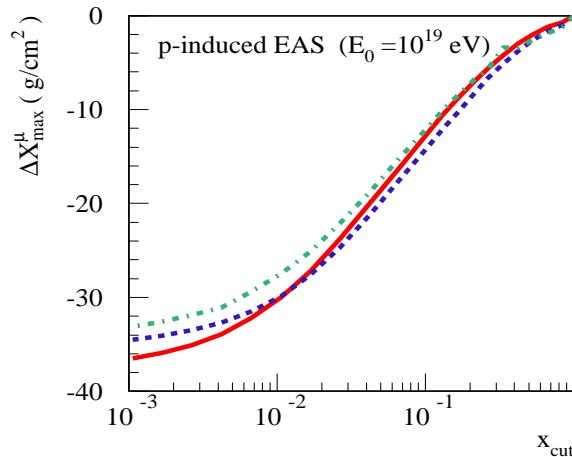


Figure 6: x_{cut} dependence for the modification of X_{max}^μ by the pion “splitting” procedure, for p -induced EAS of $E_0 = 10^{19}$ eV, for different interaction models. The meaning of the lines is the same as in Fig. 4.

10^{19} eV. Somewhat surprisingly, for this dependence, the maximal gradient is observed in almost the same x_{cut} range: of maximal importance for X_{max}^μ are secondary pions carrying few percent of the parent hadron energy. As discussed in [27], X_{max}^μ roughly corresponds to the depth in the atmosphere, where the interaction and decay lengths for most of the pions in the cascade become comparable, i.e., where the bulk of the pions approaches the pion “critical” energy. Hence, this quantity is sensitive both to the pion-air inelastic cross section and to forward production spectrum of pions. What was not properly realised in that work is that the position of that “equilibrium” point can be changed most efficiently by modifying how fast the energy partition between the produced secondary hadrons is established, thereby speeding up the decrease of the average pion energy, with increasing depth, which can again be understood using the simple Heitler’s picture for a nuclear cascade. Here, similarly to the case of N_μ , one has a competition between a copious hadron production for $x_E \rightarrow 0$ and much less numerous secondaries characterised by finite x_E , which, however, have a much stronger impact on the speed of decrease of the average pion energy. It is this competition which leads to the obtained range of pion energy fractions, corresponding to the maximal relevance for X_{max}^μ predictions. As a side remark, pion diffraction appears to have practically no impact on the predicted X_{max}^μ , contrary to what had been claimed in the literature [28] (cf. Fig. 6 for $x_{\text{cut}} \rightarrow 1$).

For completeness, we plot in Fig. 7 the x_{cut} dependence for the change of the calculated EAS maximum depth X_{max} , under such a “splitting” procedure. As one can see in the Figure, the considered modifications of secondary pion energy spectrum have a very weak impact on the predicted X_{max} , i.e., the treatment of pion-air interactions is of small importance for X_{max} predictions: even in the extreme case, $x_{\text{cut}} \rightarrow 0$, the EAS maximum depth changes by less than 5 g/cm².

To summarize this part of our analysis, both N_μ and X_{max}^μ are governed by forward pion production in hadron-air collisions: with the corresponding pion energy fractions ranging between few per cent and few tens per cent. Obviously, these conclusions can be generalized by taking into consideration the production of all “stable” hadrons, i.e., the obtained ranges of energy fractions x_E relevant for N_μ and X_{max}^μ predictions apply to the production spectra of all such hadrons.

To further support these conclusions, we plot in Fig. 8 the energy-dependence of the multiplicity

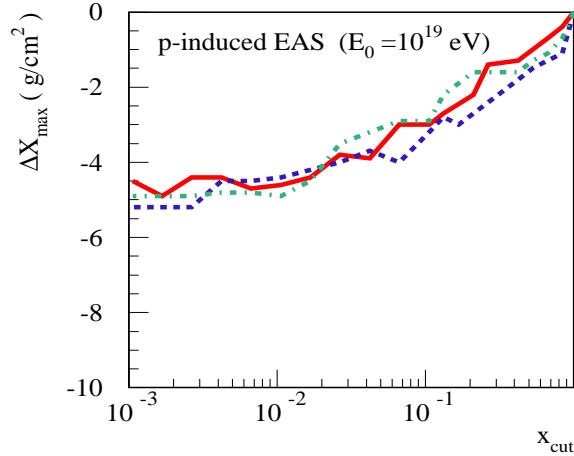


Figure 7: x_{cut} dependence for the modification of X_{max} by the pion “splitting” procedure, for p -induced EAS of $E_0 = 10^{19}$ eV, for different interaction models. The meaning of the lines is the same as in Fig. 4.

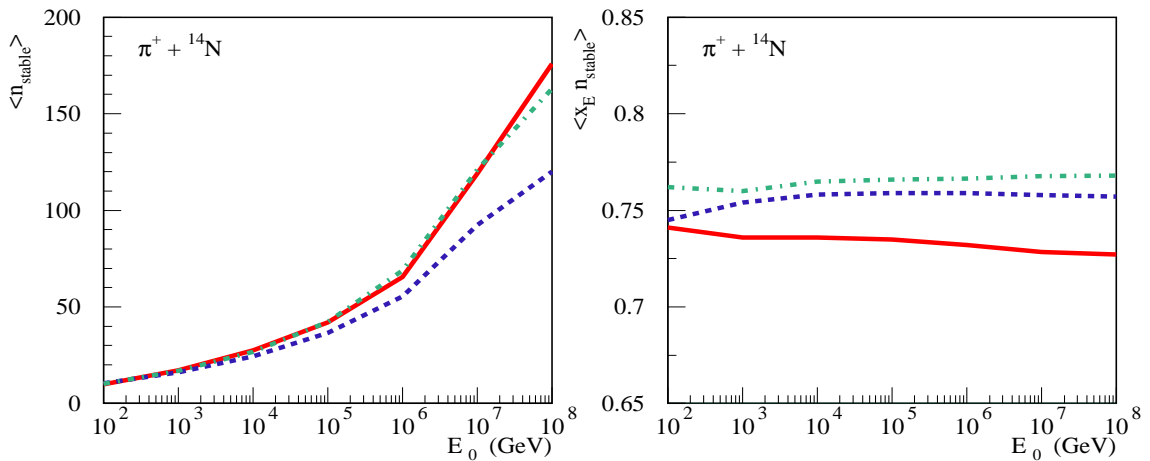


Figure 8: Energy-dependence of the multiplicity of “stable” hadrons (left) and of the energy fraction taken by all such hadrons (right) for π^+N interactions, calculated using the QGSJET-II-04, EPOS-LHC, and SIBYLL-2.3 models – solid, dashed, and dash-dotted lines, respectively.

of “stable” hadrons [(anti)nucleons, kaons, and charged pions] $\langle n_{\text{stable}}^{\pi N} \rangle$ and of the second moment of the corresponding energy fraction distribution,³ $dn_{\text{stable}}^{\pi N}/dx_E$, i.e., the average energy fraction taken by all stable secondary hadrons, for pion-nitrogen collisions,

$$\langle x_E n_{\text{stable}}^{\pi N}(E_0) \rangle = \int dx_E x_E \frac{dn_{\text{stable}}^{\pi N}(E_0, x_E)}{dx_E}, \quad (7)$$

calculated using the QGSJET-II-04, EPOS-LHC, and SIBYLL-2.3 models. As one can see in the Figure, the most steep energy rise of $\langle n_{\text{stable}}^{\pi N} \rangle$ is observed for QGSJET-II-04, while EPOS-LHC and SIBYLL-2.3 predict noticeably higher values of $\langle x_E n_{\text{stable}}^{\pi N} \rangle$ – due to a much more abundant forward production of, respectively, (anti)nucleons and ρ mesons in those models.⁴ The more abundant

³In view of some (weak) energy and model dependence of the exponent α_μ [cf. Eq. (1)], we choose to use $\langle x_E n_{\text{stable}}^{\pi N} \rangle$, instead of $\langle x_E^{\alpha_\mu} n_{\text{stable}}^{\pi N} \rangle$ considered in [23, 24].

⁴See, however, the corresponding criticism in [29].

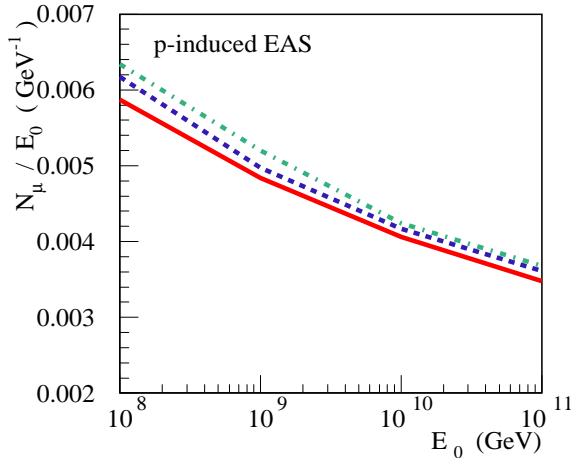


Figure 9: Dependence on primary energy of the muon number N_μ (at sea level) of proton-initiated EAS, for $E_\mu > 1$ GeV, calculated using the QGSJET-II-04, EPOS-LHC, and SIBYLL-2.3 models – solid, dashed, and dash-dotted lines, respectively.

forward production of stable hadrons in the latter two models clearly explains their somewhat higher values of the predicted N_μ , plotted in Fig. 9.

3 Potential variations of model predictions for N_μ and X_{\max}^μ

3.1 Enhancing the gluon content of the pion

As is evident from the analysis in Section 2, to increase the predicted N_μ , one has to enhance forward production of stable hadrons. Generally, there exists no viable theoretical mechanism to produce a “hardening” of secondary hadron spectra, with increasing energy: the energy-rise of multiple scattering should rather give rise to a (rather moderate) opposite effect, leading to the energy partition between larger and larger numbers of secondaries. Therefore, to obtain an enhancement of forward production, one may try to increase the multiple scattering rate in pion-air collisions, desirably, without a significant modification of the shape of forward spectra: in order to have higher secondary particle yields for all values of x_E . Since the energy-rise of multiple scattering is primarily driven by (semi)hard production processes giving rise to an emission of hadron (mini)jets, the only efficient and, probably, the only possible way to reach such a goal, without modifying substantially the treatment of proton-air collisions, rather seriously constrained by available data from the Large Hadron Collider (LHC), is to enhance the gluon content of the pion.

In principle, the fraction of the pion momentum, carried by its valence quarks, $\langle x_{q_v} \rangle$, is already strongly constrained (e.g. [30]), notably, by experimental studies of the Drell-Yan and direct photon production processes in pion-proton interactions. Therefore, one may only change the partition of the remaining momentum fraction, $1 - \langle x_{q_v} \rangle$, between gluons and sea (anti)quarks, since experimental data on pion structure functions are rather scarce and correspond to relatively large values of Bjorken x . Shifting that momentum balance towards gluons, at the expense of sea (anti)quarks, would enhance the multiple scattering rate: because gluons participate in hard scattering with a larger color factor, $C_A = 3$, compared to $C_F = 4/3$ of (anti)quarks.

Here we wish to study an extreme variation of the glue in the pion. Therefore, we choose to modify the overall momentum fraction possessed by both gluons and sea (anti)quarks, $\langle x_g \rangle + \langle x_{q_s} \rangle$, at the expense of $\langle x_{q_v} \rangle$. I.e., for the moment, we disregard the respective experimental constraints

and consider a factor of two reduction of $\langle x_{q_v} \rangle$,⁵ while enhancing correspondingly both $\langle x_g \rangle$ and $\langle x_{q_s} \rangle$. This way we change the gluon PDF rather radically in the x -range relevant for N_μ and X_{\max}^μ predictions, as demonstrated in Fig. 10.

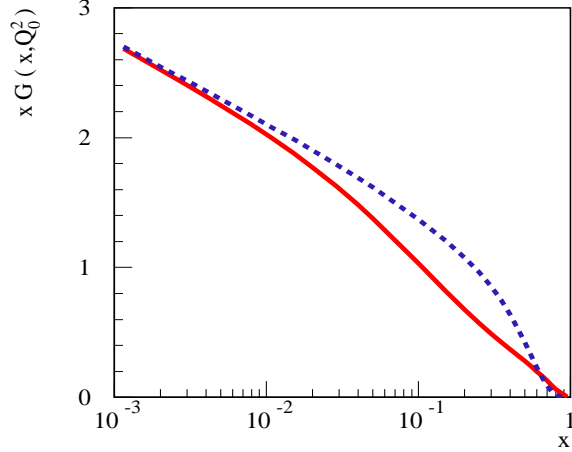


Figure 10: Gluon PDF of the pion at $Q_0^2 = 2 \text{ GeV}^2$ in the default QGSJET-III model (solid line) and for the enhanced gluon content of the pion, as discussed in the text (dashed line).

Yet, as one can see in Fig. 11 (left), such a modification gives rise to a noticeably higher

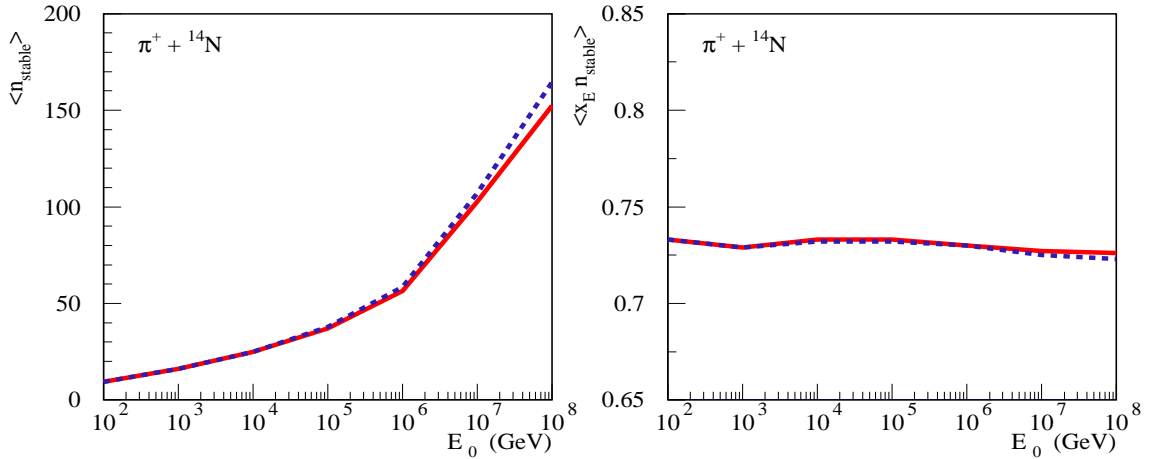


Figure 11: Energy-dependence of the multiplicity of “stable” hadrons (left) and of the energy fraction taken by all such hadrons (right) for π^+N interactions, for the default QGSJET-III model (solid line) and for the enhanced gluon content of the pion, as discussed in the text (dashed line).

multiplicity of stable secondary hadrons $\langle n_{\text{stable}}^{\pi N} \rangle$, for pion-nitrogen collisions, only at the highest energies considered. Moreover, the average fraction of the parent pion energy, taken by all such

⁵This is achieved by modifying the original GRS parton distribution functions (PDFs) of valence quarks in the pion [30], employed in the QGSJET-III model, at the cutoff scale $Q_0^2 = 2 \text{ GeV}^2$ for hard processes, by a factor $A_\delta(1-x)^\delta$, and choosing the parameters δ and A_δ in such a way that the desirable reduction of $\langle x_{q_v} \rangle$ is obtained without violating the valence quark sum rule. Additionally, we increase the value of the parameter β_π governing the “hardness” of the gluon PDF in QGSJET-III ($\propto (1-x)^{\beta_\pi}$ – cf. Eq. (8) in [12]), from the default value 2 to 5, in order to shift the enhancement of the glue towards smaller x . PDFs at higher virtuality scales q^2 are obtained via a DGLAP evolution from Q_0^2 to q^2 .

hadrons, $\langle x_E n_{\text{stable}}^{\pi N} \rangle$, remains practically unaffected, see Fig. 11 (right), which means that the considered modification has a minor impact on forward hadron spectra. Not surprisingly, applying the so-modified treatment of pion-air interactions to EAS modeling, we observed rather insignificant changes for the calculated EAS muon content and for the maximal muon production depth, compared to QGSJET-III predictions ($\lesssim 1\%$ for N_μ and few g/cm^2 for X_{max}^μ).

3.2 Modifying the model calibration to experimental data

An alternative way to increase the predicted N_μ is to enhance the yields of stable secondary hadrons, at the expense of neutral pions. In relation to that, let us pay attention to the fact that the QGSJET-III model seriously underestimates the production of kaons and (anti)nucleons in π^-C collisions, compared to measurements by the NA61 experiment [26], as one can see in Figs. 12 and 13 (solid lines). The agreement with the data can be improved performing suitable modifications

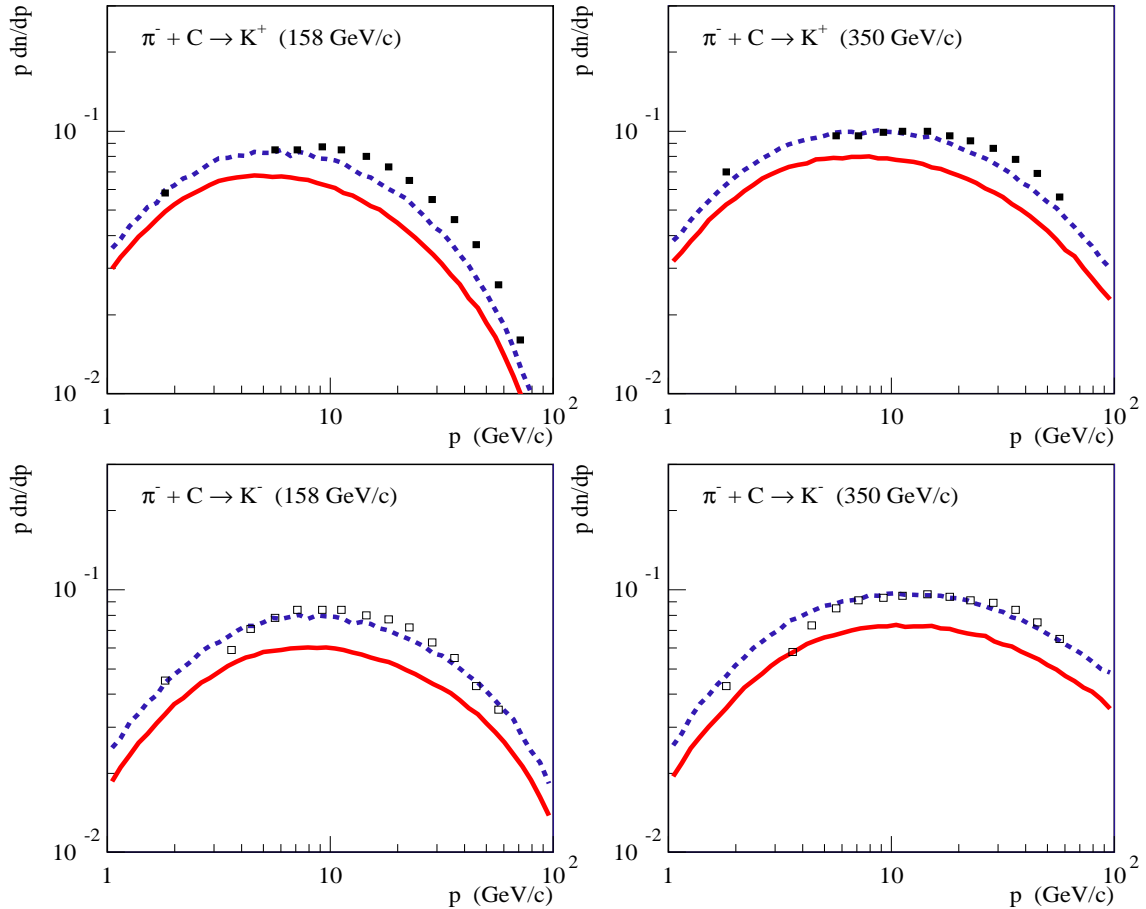


Figure 12: Momentum distributions (in lab. frame) of K^+ (top panels) and K^- (bottom panels) produced in π^-C collisions at 158 GeV/c (left) and 350 GeV/c (right), as calculated using the default QGSJET-III model (solid lines) or considering an enhancement of kaon production, as discussed in the text (dashed lines), compared to NA61 data [26] (points).

of the hadronization procedure of the model: considering, respectively, 40% increase for the probability to create strange quark-antiquark ($s\bar{s}$) pairs from the vacuum or 60% enhancement of the corresponding probability for diquark-antidiquark ($ud\bar{u}\bar{d}$) pairs, when treating the hadronization of strings of color field, stretched between final partons produced [13], the corresponding results

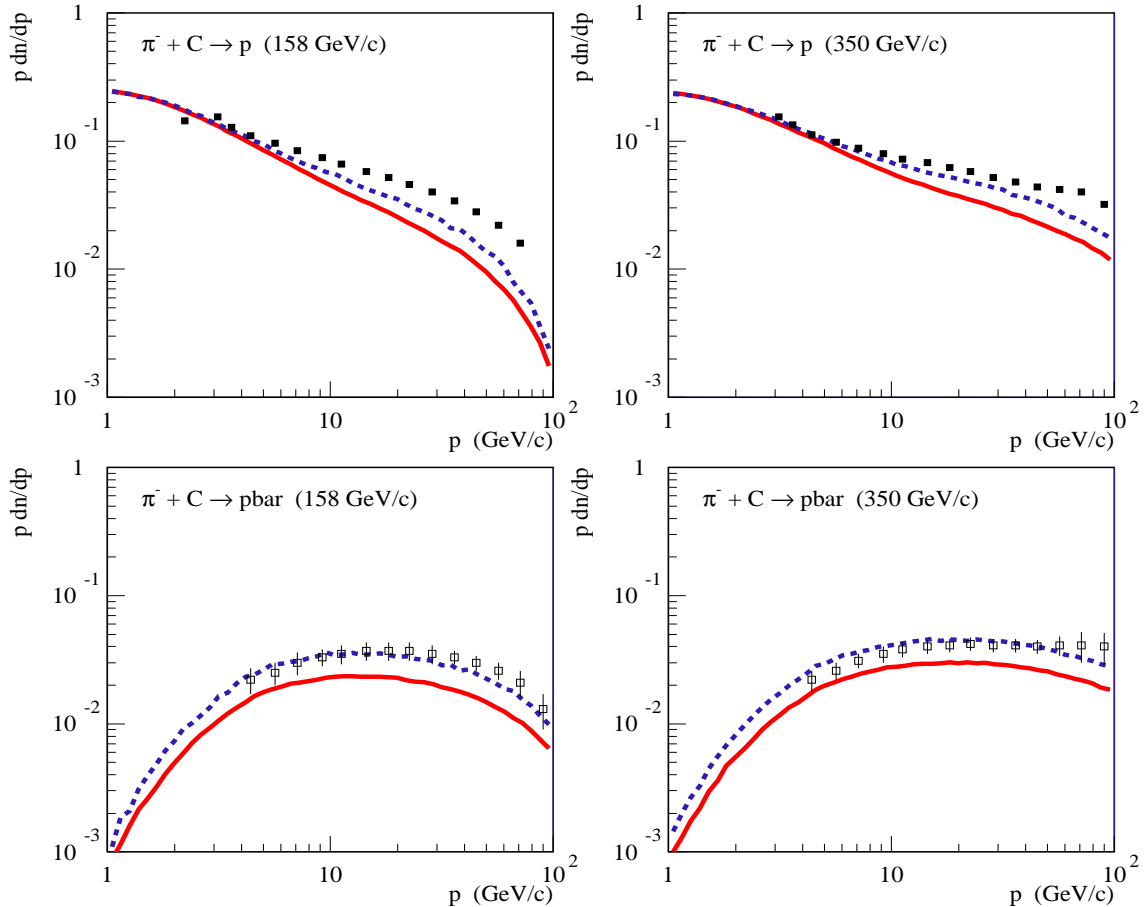


Figure 13: Momentum distributions (in lab. frame) of protons (top panels) and antiprotons (bottom panels) produced in π^- -C collisions at 158 GeV/c (left) and 350 GeV/c (right), as calculated using the default QGSJET-III model (solid lines) or considering an enhancement of (anti)nucleon production, as discussed in the text (dashed lines), compared to NA61 data [26] (points).

being shown in Figs. 12 and 13 by dashed lines. On the other hand, the agreement with NA61 data on ρ^0 meson production [31] can be further improved considering 50% enhancement for the probability of the fragmentation of light (anti)quarks into ρ mesons, compared to the default value $1/3$ used in the model, see Fig. 14.

It is noteworthy, however, that the considered enhancements of kaon and (anti)nucleon production are at tension with the corresponding data on pion-proton collisions from other experiments, as one can see, e.g., in Fig. 15. Moreover, since the hadronization procedure is universal for all kinds of hadronic interactions, such changes lead to a strong contradiction with the corresponding particle yields measured in pp interactions, both at fixed target energies and at LHC (see [13] for a comparison of the default QGSJET-III results with such data). In turn, for the considered enhancement of ρ meson production, the fraction of directly produced pions falls down to $\simeq 30\%$, in a clear contradiction to observations [33].

Regarding the impact on EAS muon content, the considered enhancements of kaon and (anti)nucleon production give rise up to $\sim 10\%$ increase of the predicted N_μ , compared to the original results of QGSJET-III, as one can see in Fig. 16 (left). On the other hand, the considered increase of ρ meson yield appears to have only a minor effect: $\Delta N_\mu/N_\mu < 1\%$, which is a direct consequence

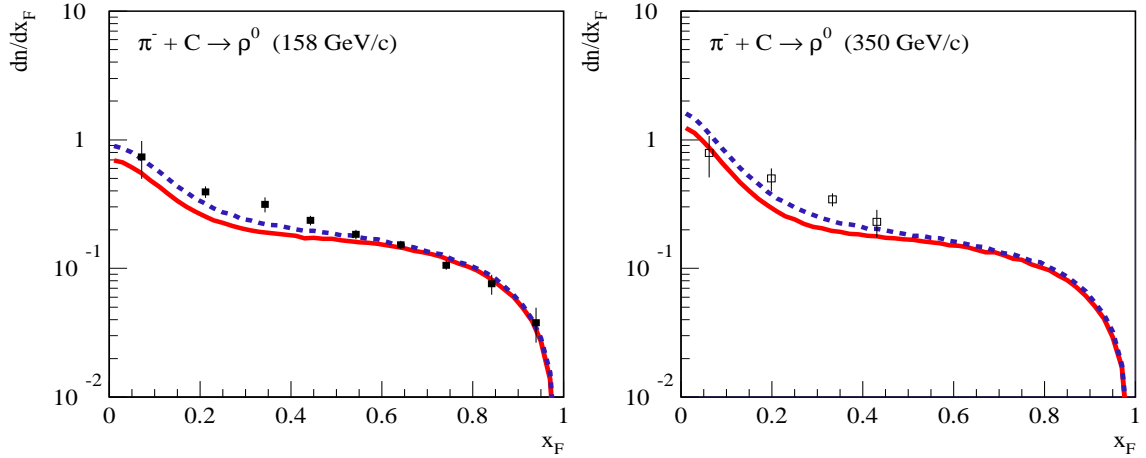


Figure 14: Feynman x distributions (in c.m. frame) of ρ^0 mesons produced in π^-C collisions at 158 GeV/c (left) and 350 GeV/c (right), as calculated using the default QGSJET-III model (solid lines) or considering an enhancement of ρ meson production, as discussed in the text (dashed lines), compared to NA61 data [31] (points).

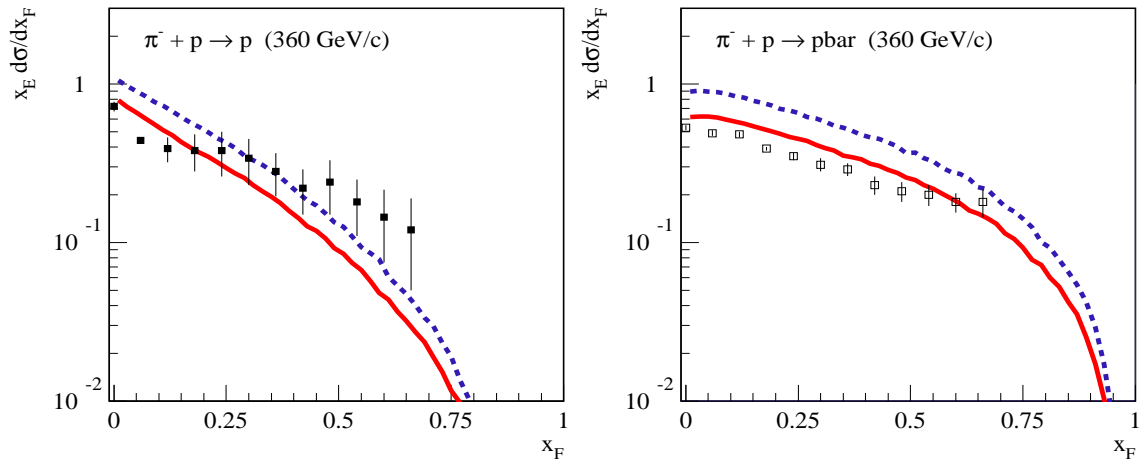


Figure 15: Feynman x distributions (in c.m. frame) of protons (left) and antiprotons (right) in π^-p collisions at 360 GeV/c, as calculated using the default QGSJET-III model (solid lines) or considering an enhancement of (anti)nucleon production, as discussed in the text (dashed lines), compared to LEBC-EHS data [32] (points).

of the isospin symmetry.⁶ Indeed, since such an enhancement of ρ meson production does not modify the energy partition between nuclear and e/m subcascades initiated by the, respectively, charged and neutral pions resulting from decays of ρ mesons, we are essentially back to the picture discussed in Section 2. Then, since this enhancement of ρ meson yield mainly affects central (in c.m. frame) production characterized by small energy fractions x_E of the mesons, at sufficiently high energies, it is of minor importance for N_μ predictions, as demonstrated in Section 2.

The effect of the considered modifications of particle production on the calculated maximal muon production depth X_{\max}^μ is shown in Fig. 16 (right). Enhancing the yields of secondary kaons

⁶While the isospin symmetry is not exact for strong interactions, it holds to a very good accuracy thanks to the small mass difference between u and d quarks.

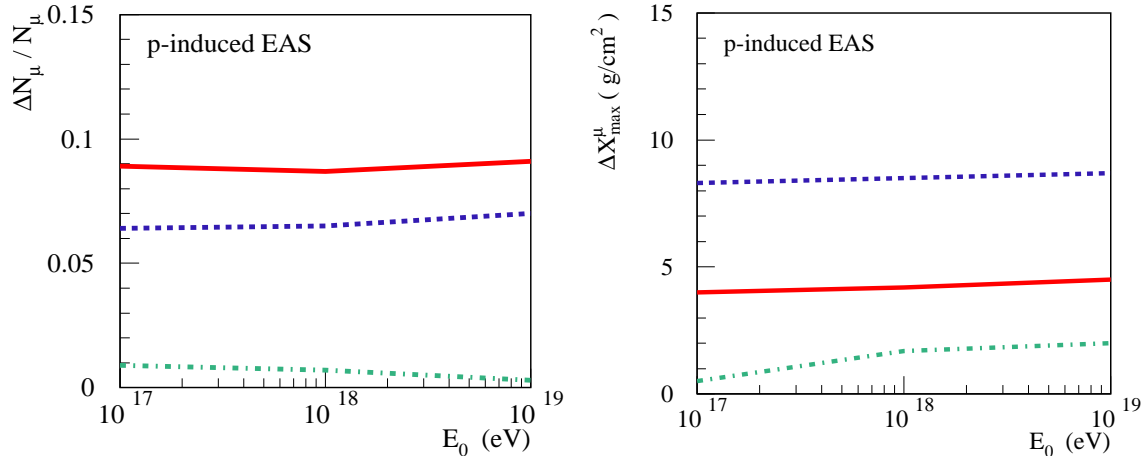


Figure 16: Energy dependence of the relative change of the muon number N_μ at sea level (left) and of the modification of the maximal muon production depth X_{\max}^μ (right), both for $E_\mu > 1$ GeV, for proton-initiated EAS, with respect to the corresponding predictions of the default QGSJET-III model, for the considered modifications of the model: enhancement of (anti)nucleon, kaon, and ρ meson production – solid, dashed, and dash-dotted lines, respectively.

and (anti)nucleons, one shifts the energy balance between hadronic and e/m subcascades in favor of the former, thereby slowing down the energy “leak” from the hadronic component of extensive air showers and elongating the nuclear cascade, as discussed in some detail in [27]. The corresponding values of X_{\max}^μ exceed the ones of the original QGSJET-III by up to ~ 10 g/cm². On the other hand, the considered increase of ρ meson production has a much weaker impact on X_{\max}^μ .

3.3 Changing the energy-dependence of the pion exchange process

The very last remaining option regarding a potentially strong enhancement of EAS muon content is related to pion exchange process in pion-air collisions, i.e., to the so-called Reggeon-Reggeon-Pomeron ($\mathbb{R}\mathbb{R}\mathbb{P}$) contribution, with $\mathbb{R} = \pi$, to secondary hadron production. As discussed in [18], assuming a dominance of the pion exchange in the $\mathbb{R}\mathbb{R}\mathbb{P}$ configuration, due to the small pion mass, compared to other Reggeons, one obtains $\simeq 20\%$ enhancement of N_μ , relative to the case when this contribution is neglected. This is because such a process changes the energy balance between secondary charged and neutral pions in favor of the former. Indeed, the dominant decay channels $\rho^\pm \rightarrow \pi^\pm \pi^0$ and $\rho^0 \rightarrow \pi^+ \pi^-$ give rise to

$$\langle x_{\pi^\pm}^{\mathbb{R}\mathbb{R}\mathbb{P}} \rangle : \langle x_{\pi^0}^{\mathbb{R}\mathbb{R}\mathbb{P}} \rangle = 3:1, \quad (8)$$

for the products of forward ρ meson decays, in contrast to $\langle x_{\pi^\pm} \rangle : \langle x_{\pi^0} \rangle = 2:1$ for the usual (“central”) ρ meson production discussed in Section 3.2.

However, the energy-dependence of that contribution depends crucially on the treatment of absorptive effects defining the probability for the corresponding “rapidity gap survival”, i.e., that the (small) rapidity gap between the leading hadron (here, ρ meson) and other secondary particles produced by an interaction of the virtual pion with the target nucleus, is not filled by particle production due to additional multiple scattering processes [18, 29, 34, 35, 36].

Here we are going to consider an extreme case: neglecting such absorptive corrections and assuming that the pion exchange process constitutes a fixed fraction w_π^{lim} of the inelastic cross section. I.e., for any inelastic pion-air collision, we consider with the probability w_π^{lim} a production of a charged or neutral ρ meson, with equal probabilities (e.g. [37]), sampling its light cone momentum fraction x and transverse momentum p_t according to the corresponding probability

$f_{\pi\text{-air}}(x, p_t^2)$ for reggeized pion exchange in the Born approximation (e.g. [38]), while treating the rest of hadron production for the event as an interaction of the virtual pion with air nucleus. Here

$$f_{\pi\text{-air}}(x, p_t^2) \propto \frac{xt}{(t - m_\pi^2)^2} F^2(t)(1-x)^{1-2\alpha_\pi(t)} \sigma_{\pi\text{-air}}^{\text{tot}}((1-x)s), \quad (9)$$

with the squared momentum transfer t being related to p_t as

$$-t = p_\perp^2/x + (1-x)(m_\rho^2/x - m_\pi^2). \quad (10)$$

$\alpha_\pi(t) = \alpha'_\pi(t - m_\pi^2)$ is the pion Regge trajectory with the slope $\alpha'_\pi \simeq 0.9 \text{ GeV}^{-2}$, $\sigma_{\pi\text{-air}}^{\text{tot}}$ is the total pion-air cross section,⁷ $F(t)$ is the pion emission form factor,⁸ m_π and m_ρ are the pion and ρ meson masses, respectively, and s is the c.m. energy for the interaction.

Choosing $w_\pi^{\text{lim}}=0.11$, based on the data of the NA61 experiment [31], see Fig. 17, the resulting spectrum of ρ^0 mesons and the partial contribution of the pion exchange process for pion-nitrogen

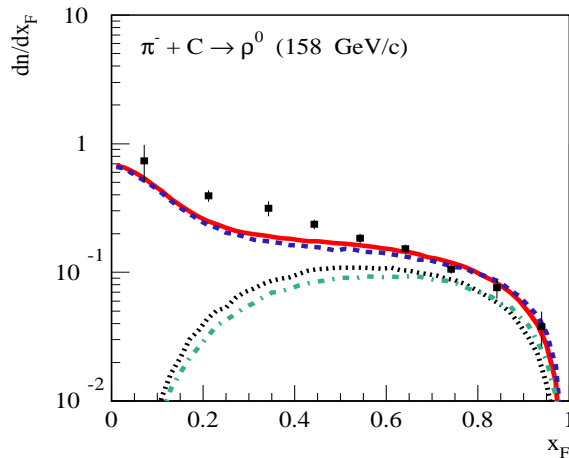


Figure 17: Feynman x distribution (in c.m. frame) of ρ^0 mesons produced in π^- C collisions at 158 GeV/c, calculated using the default QGSJET-III model (solid line) or applying the alternative treatment for the pion exchange process, as discussed in the text (dashed line). The corresponding partial contributions of the pion exchange process are shown by dotted and dash-dotted lines, respectively.

collisions at 1 PeV are shown in Fig. 18, in comparison to the corresponding predictions of QGSJET-III. In turn, the obtained energy-dependence of the relative change of N_μ , corresponding to this alternative treatment, is plotted in Fig. 19 (left).

Somewhat surprisingly, such a treatment results in a lower muon number, compared to the predictions of the default QGSJET-III model. To understand this nontrivial result, let us remind ourselves that a considerable part of the cross section $\sigma_{\pi\text{-air}}^{\text{tot}}$ in Eq. (9) corresponds to elastic scattering (see Fig. 20),

$$\sigma_{\pi\text{-air}}^{\text{tot}} = \sigma_{\pi\text{-air}}^{\text{el}} + \sigma_{\pi\text{-air}}^{\text{inel}}, \quad (11)$$

with the corresponding fraction $\sigma_{\pi\text{-air}}^{\text{el}}/\sigma_{\pi\text{-air}}^{\text{tot}}$ being $\sim 30\%$ at fixed target energies and slowly rising with E_0 , approaching the “black disk” limit ($\sigma_{\pi\text{-air}}^{\text{el}}/\sigma_{\pi\text{-air}}^{\text{tot}} \rightarrow 0.5$) in the $E_0 \rightarrow \infty$ limit. For that elastic scattering contribution, the final state consists of a ρ meson and a pion only: with the

⁷Since the scattering proceeds close to the pion pole, it is characterized by relatively small momentum transfer squared t , i.e., we deal with quasi-real pions. Therefore, for $\sigma_{\pi\text{-air}}^{\text{tot}}$ and for its decomposition into inelastic and elastic parts, Eq. (11), we use the results of QGSJET-III, corresponding to the usual pion-nucleus interaction.

⁸Since the precise form of this form factor is of minor importance for the current study, we use the one for $pp \rightarrow nX$ reaction, $F(t) = \exp(R_\pi^2 t/2)$, with $R_\pi^2 \simeq 0.3 \text{ GeV}^{-2}$ [34].

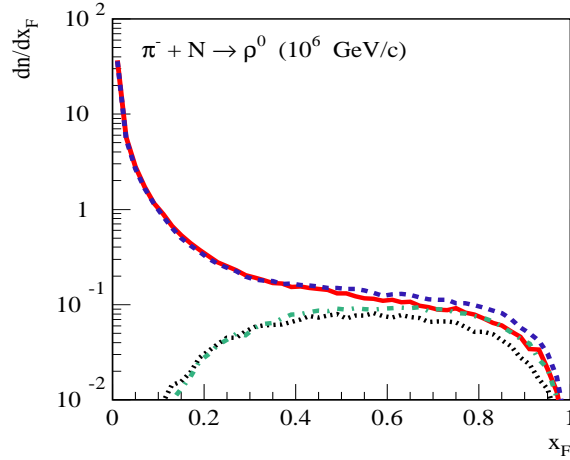


Figure 18: Same as in Fig. 17, in π^- -N collisions at 1 PeV.

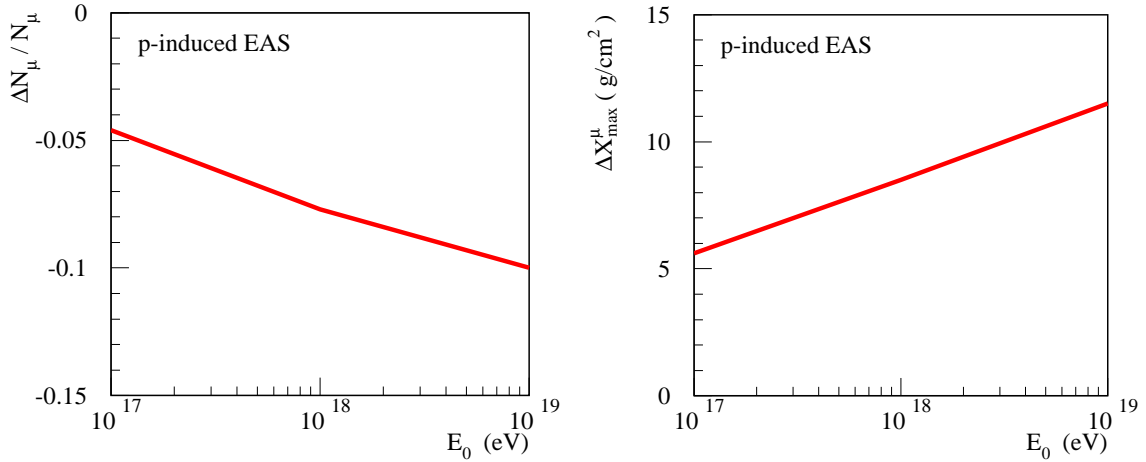


Figure 19: Energy dependence of the relative change of the muon number N_μ at sea level (left) and of the modification of the maximal muon production depth X_{\max}^μ (right), both for $E_\mu > 1$ GeV, for proton-initiated EAS, with respect to the corresponding predictions of the default QGSJET-III model, for the alternative treatment of the pion exchange process, discussed in the text.

virtual pion being put on-shell by the scattering process, see Fig. 20 (right). It is such a scarce hadron production which gives rise to the obtained decrease of N_μ .

In contrast, in the treatment of the QGSJET-III model, the rise of absorptive corrections “pushes” the pion exchange process towards larger and larger impact parameters, causing a (slow) decrease of its relative contribution [29, 36]. At the same time, at large impact parameters, the above-discussed contribution of elastic scattering of the virtual pion is strongly suppressed and can be neglected [36].

Regarding the maximal muon production depth, in addition to a scarce hadron production in case of elastic scattering of the virtual pion, one has a shift of the energy balance between hadronic and e/m subcascades in favor of the former [cf. Eq. (8)], both effects contributing to an elongation of the nuclear cascade profile. The resulting X_{\max}^μ values exceed the ones of the original QGSJET-III by up to ~ 10 g/cm², see Fig. 19 (right).

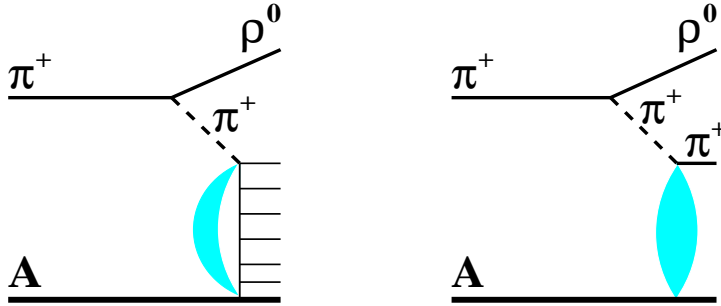


Figure 20: Schematic view of the two contributions to the pion exchange process: for inelastic scattering of the virtual pion (left), the leading ρ meson is accompanied by multiple hadron production; elastic scattering (right) gives rise to only one secondary pion, in addition to the ρ meson. The light shaded croissant and ellipsis correspond to contributions of elastic rescattering processes.

4 Conclusions

In this work, we investigated the possibility to increase the predicted EAS muon content, within the framework of the QGSJET-III model, restricting ourselves to the standard physics picture. We started with specifying the kinematic range for secondary hadron production, which is of relevance for model predictions regarding the muon number N_μ and the maximal muon production depth X_{\max}^μ , and demonstrated that these quantities are governed by forward pion production in hadron-air collisions: with the corresponding pion energy fractions, taken from their parent hadrons, ranging between few percent and few tens of percent. Further, we investigated the impact on the predicted N_μ and X_{\max}^μ of various modifications of the treatment of hadronic interactions, in particular the model calibration to accelerator data, the amount of the “glue” in the pion, and the energy dependence of the pion exchange process.

The strongest N_μ enhancement reaching 10% level has been obtained when we increased the yields of secondary kaons and (anti)nucleons in the model, adjusting its predictions to NA61 data on pion-carbon interactions at fixed target energies. However, such modifications should be considered as extreme ones, since they lead to a serious tension with results of other experiments, regarding the yields of such hadrons both in pion-proton and, especially, in proton-proton collisions.

As for the gluon content of the pion, even considering extreme changes of the momentum partition between valence quarks and gluons, we obtained no noticeable effects for the predicted N_μ and X_{\max}^μ . This is because such changes impact pion-air collisions at the highest energies only, in the atmospheric nuclear cascade, while being of minor importance for the bulk of such interactions at lower energies, at later stages of the cascade development.

Regarding the pion exchange process in pion-air collisions, the (slow) decrease with energy of the corresponding probability can only be tamed if one assumes that absorptive corrections to the process are rather weak. However, in such a case, a significant part of the cross section for the virtual pion interaction with the target nucleus corresponds to elastic scattering. The corresponding very scarce hadron production results in a decrease of the predicted N_μ .

Regarding X_{\max}^μ , for some of the considered modifications of particle production, we obtained up to ~ 10 g/cm² changes of the maximal muon production depth, typically yielding larger values of X_{\max}^μ . This aggravates the tension with observations of the Pierre Auger Observatory.

Overall, we see no possibility to increase the predicted EAS muon content by more than 10%, without entering in a serious contradiction with relevant accelerator data, while staying within the standard physics picture.

Acknowledgments

The work of S.O. was supported by Deutsche Forschungsgemeinschaft (project number 465275045). G.S. acknowledges support by the Bundesministerium für Bildung und Forschung, under grants 05A20GU2 and 05A23GU3.

References

- [1] M. Nagano and A. A. Watson, *Observations and implications of the ultrahigh-energy cosmic rays*, Rev. Mod. Phys. **72**, 689 (2000).
- [2] R. Engel, D. Heck and T. Pierog, *Extensive air showers and hadronic interactions at high energy*, Ann. Rev. Nucl. Part. Sci. **61**, 467 (2011).
- [3] A. Aab *et al.* (Pierre Auger Collaboration), *Muons in Air Showers at the Pierre Auger Observatory: Mean Number in Highly Inclined Events*, Phys. Rev. D **91** (2015) 032003.
- [4] A. Aab *et al.* (Pierre Auger Collaboration), *Testing Hadronic Interactions at Ultrahigh Energies with Air Showers Measured by the Pierre Auger Observatory*, Phys. Rev. Lett. **117**, 192001 (2016).
- [5] A. Abdul Halim *et al.* (Pierre Auger Collaboration), *Testing Hadronic-Model Predictions of Depth of Maximum of Air-Shower Profiles and Ground-Particle Signals using Hybrid Data of the Pierre Auger Observatory*, [arXiv:2401.10740 [astro-ph.HE]].
- [6] R.U. Abbasi *et al.* (Telescope Array Collaboration), *Study of muons from ultrahigh energy cosmic ray air showers measured with the Telescope Array experiment*, Phys. Rev. D **98**, 022002 (2018).
- [7] J. Albrecht, L. Cazon, H. Dembinski, A. Fedynitch, and K.-H. Kampert, *The Muon Puzzle in cosmic-ray induced air showers and its connection to the Large Hadron Collider*, Astrophys. Space Sci. **367**, 27 (2022).
- [8] G. R. Farrar and J. D. Allen, *A new physical phenomenon in ultra-high energy collisions*, EPJ Web Conf. **53**, 07007 (2013).
- [9] L. A. Anchordoqui, H. Goldberg, and T. J. Weiler, *Strange fireball as an explanation of the muon excess in Auger data*, Phys. Rev. D **95** (2017) 063005.
- [10] T. Pierog, S. Baur, H. Dembinski, M. Perlin, R. Ulrich, and K. Werner, *When heavy ions meet cosmic rays: potential impact of QGP formation on the muon puzzle*, PoS (ICRC2021), 469 (2021).
- [11] J. Manshanden, Günter Sigl, and M. V. Garzelli, *Modeling strangeness enhancements to resolve the muon excess in cosmic ray extensive air shower data*, JCAP **02**, 017 (2023).
- [12] S. Ostapchenko, *QGSJET-III model of high energy hadronic interactions: The formalism*, Phys. Rev. D **109**, 034002 (2024).
- [13] S. Ostapchenko, *QGSJET-III model of high energy hadronic interactions: II. Particle production and extensive air shower characteristics*, [arXiv:2403.16106 [hep-ph]].
- [14] A. Aab *et al.* (Pierre Auger Collaboration), *Muons in Air Showers at the Pierre Auger Observatory: Measurement of Atmospheric Production Depth*, Phys. Rev. D **90**, 012012 (2014).
- [15] L. Collica (Pierre Auger Collaboration), *Measurement of the Muon Production Depths at the Pierre Auger Observatory*, Eur. Phys. J. Plus **131**, no.9, 301 (2016) doi:10.1140/epjp/i2016-16301-6 [arXiv:1609.02498 [astro-ph.HE]].

- [16] R. Ulrich, R. Engel and M. Unger, *Hadronic Multiparticle Production at Ultra-High Energies and Extensive Air Showers*, Phys. Rev. D **83**, 054026 (2011).
- [17] S. Ostapchenko, *Monte Carlo treatment of hadronic interactions in enhanced Pomeron scheme: QGSJET-II model*, Phys. Rev. D **83**, 014018 (2011).
- [18] S. Ostapchenko, *QGSJET-II: physics, recent improvements, and results for air showers*, EPJ Web Conf. **52**, 02001 (2013).
- [19] T. Pierog, Iu. Karpenko, J. M. Katzy, E. Yatsenko, and K. Werner, *EPOS LHC: Test of collective hadronization with data measured at the CERN Large Hadron Collider*, Phys. Rev. C **92**, 034906 (2015).
- [20] F. Riehn, R. Engel, A. Fedynitch, T. K. Gaisser, and T. Stanev, *Hadronic interaction model Sibyll 2.3d and extensive air showers*, Phys. Rev. D **102**, 063002 (2020).
- [21] W. Heitler, *The Quantum Theory of Radiation*, Oxford University Press (1954).
- [22] J. Matthews, *A Heitler model of extensive air showers*, Astropart. Phys. **22**, 387 (2005).
- [23] A. M. Hillas, *Shower simulation: Lessons from MOCCA*, Nucl. Phys. B Proc. Suppl. **52**, 29 (1997).
- [24] M. Reininghaus, R. Ulrich, and T. Pierog, *Air shower genealogy for muon production*, PoS (ICRC2021), 463 (2021).
- [25] T. Bergmann, R. Engel, D. Heck, N. N. Kalmykov, S. Ostapchenko, T. Pierog, T. Thouw, and K. Werner, *One-dimensional Hybrid Approach to Extensive Air Shower Simulation*, Astropart. Phys. **26**, 420 (2007).
- [26] H. Adhikary *et al.* (NA61/SHINE Collaboration), *Measurement of hadron production in π^- -C interactions at 158 and 350 GeV/c with NA61/SHINE at the CERN SPS*, Phys. Rev. D **107**, 062004 (2023).
- [27] S. Ostapchenko and M. Bleicher, *Constraining pion interactions at very high energies by cosmic ray data*, Phys. Rev. D **93**, 051501(R) (2016).
- [28] T. Pierog, *Open issues in hadronic interactions for air showers*, EPJ Web Conf. **145**, 18002 (2017).
- [29] S. Ostapchenko, *Cosmic ray interactions in the atmosphere: QGSJET-III and other models*, SciPost Phys. Proc. **13**, 004 (2023).
- [30] M. Gluck, E. Reya, and I. Schienbein, *Pionic parton distributions revisited*, Eur. Phys. J. C **10**, 313 (1999).
- [31] A. Aduszkiewicz *et al.* (NA61/SHINE Collaboration), *Measurement of meson resonance production in π^- -C interactions at SPS energies*, Eur. Phys. J. C **77**, 626 (2017).
- [32] M. Aguilar-Benitez *et al.* (LEBC-EHS Collaboration), *Longitudinal Distribution of π^\pm , K^\pm , Protons and Anti-protons Produced in 360-GeV/c π^-p Interactions*, Europhys. Lett. **4**, 1261 (1987).
- [33] M. Aguilar-Benitez *et al.* (LEBC-EHS Collaboration), *Vector meson production in π^-p interactions at 360-GeV/c*, Z. Phys. C **44**, 531 (1989).
- [34] B. Z. Kopeliovich, I. K. Potashnikova, Ivan Schmidt, H. J. Pirner, and K. Reygers, *Pion-pion cross section from proton-proton collisions at LHC*, Phys. Rev. D **91**, 054030 (2015).

- [35] V. A. Khoze, A. D. Martin, and M. G. Ryskin, *Total π^+p cross section extracted from the leading neutron spectra at the LHC*, Phys. Rev. D **96**, 034018 (2017).
- [36] S. Ostapchenko, *QGSJET-III model: novel features*, Phys. At. Nucl. **44**, 1017 (2021).
- [37] G. G. Arakelyan, N. Ya. Ivanov, and A. A. Grigoryan, *Inclusive production of ρ resonances in πN interactions: A Theoretical analysis*, Z. Phys. C **52**, 317 (1991).
- [38] A. B. Kaidalov, V. A. Khoze, A. D. Martin, and M. G. Ryskin, *Leading neutron spectra*, Eur. Phys. J. C **47**, 385 (2006).